Article
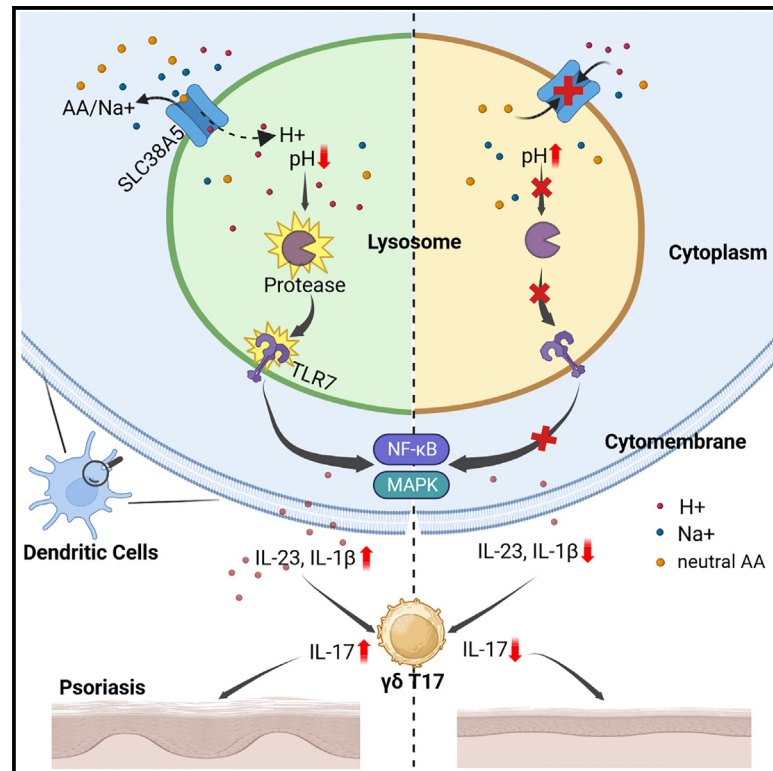
SLC38A5 aggravates DC-mediated psoriasiform skin inflammation via potentiating lysosomal acidification

Graphical abstract

Highlights

- Neutral amino acid transporter SLC38A5 potentiates psoriatic skin inflammation

- SLC38A5 is mainly distributed in dermal dendritic cells of psoriatic skin tissues

- SLC38A5 locates on lysosome to facilitate its acidification

- SLC38A5 promotes TLR7 signaling activation and pro-inflammatory cytokine production

Authors

Leqing Zhu, Xichun Xia, Guangqiang Li, ...,
Lianghua Bin, Guangchao Cao, Zhinan Yin

Correspondence

wangqian@jnu.edu.cn (Q.W.),
liehuadeng@126.com (L.D.),
lianghuab@yahoo.com (L.B.),
gccao2016@jnu.edu.cn (G.C.),
tzhinan@jnu.edu.cn (Z.Y.)

In brief

Zhu et al. show that SLC38A5, a sodium-dependent neutral aa transporter that counter-transports protons, locates on the lysosome of dermal dendritic cells and facilitates lysosomal acidification. SLC38A5 promotes the activation of TLR7 signaling and the production of pro-inflammatory cytokines from dermal dendritic cells, therefore potentiating psoriatic skin inflammation.

CellPress

Article

SLC38A5 aggravates DC-mediated psoriasiform skin inflammation via potentiating lysosomal acidification

Leqing Zhu,[1,3,4,11] Xichun Xia,[1,2,11] Guangqiang Li,[1,11] Chuyun Zhu,[1,2,11] Qingqing Li,[5] Baocheng Wang,[6] Nan-Xi Shi,[1] Zhiwei Lei,[7,8] Shuxian Yang,[1] Zhanpeng Zhang,[3] Haishan Li,[1] Jingyi Tan,[1,2] Zonghua Liu,[1] Qiong Wen,[1,2] Hui Zhong,[1,2] Xue-Jia Lin,[1,2] Guodong Sun,[9] Xiucong Bao,[10] Qian Wang,[1,2,*] Liehua Deng,[3,*] Lianghua Bin,[1,*] Guangchao Cao,[1,2,*] and Zhinan Yin[1,2,12,*]

[1]The Biomedical Translational Research Institute, Key Laboratory of Ministry of Education for Viral Pathogenesis & Infection Prevention and Control, Health Science Center (School of Medicine), Jinan University, Guangzhou 510632, China
[2]Guangdong Provincial Key Laboratory of Tumor Interventional Diagnosis and Treatment, Zhuhai Institute of Translational Medicine, Zhuhai People's Hospital Affiliated with Jinan University, Jinan University, Zhuhai 519000, China
[3]Department of Dermatology, First Affiliated Hospital, Health Science Center (School of Medicine), Jinan University, Guangzhou 510632, China
[4]Guangzhou National Laboratory, Guangzhou International BioIsland, Guangzhou 510005, China
[5]Department of Dermatology, Guangdong Women's and Children's Hospital, Guangzhou 511442, China
[6]Tsinghua-Berkeley Shenzhen Institute, Tsinghua University, Shenzhen 518055, China
[7]The Sixth Affiliated Hospital of Guangzhou Medical University, Qingyuan People's Hospital, Qingyuan 511518, China
[8]Guangdong Provincial Key Laboratory of Virology, Institute of Medical Microbiology, Jinan University, Guangzhou 510632, China
[9]Guandgong Provincial Key Laboratory of Spine and Spinal Cord Reconstruction, The Fifth Affiliated Hospital (Heyuan Shenhe People's Hospital), Jinan University, Heyuan 517000, China
[10]School of Biomedical Sciences, Li Ka Shing Faculty of Medicine, The University of Hong Kong, Hong Kong SAR, China
[11]These authors contributed equally
[12]Lead contact
*Correspondence: wangqian@jnu.edu.cn (Q.W.), liehuadeng@126.com (L.D.), lianghuab@yahoo.com (L.B.), gccao2016@jnu.edu.cn (G.C.), tzhinan@jnu.edu.cn (Z.Y.)
https://doi.org/10.1016/j.celrep.2023.112910

SUMMARY

Amino acid (aa) metabolism is closely correlated with the pathogenesis of psoriasis; however, details on aa transportation during this process are barely known. Here, we find that SLC38A5, a sodium-dependent neutral aa transporter that counter-transports protons, is markedly upregulated in the psoriatic skin of both human patients and mouse models. SLC38A5 deficiency significantly ameliorates the pathogenesis of psoriasis, indicating a pathogenic role of SLC38A5. Surprisingly, SLC38A5 is almost exclusively expressed in dendritic cells (DCs) when analyzing the psoriatic lesion and mainly locates on the lysosome. Mechanistically, SLC38A5 potentiates lysosomal acidification, which dictates the cleavage and activation of TLR7 with ensuing production of pro-inflammatory cytokines such as interleukin-23 (IL-23) and IL-1β from DCs and eventually aggravates psoriatic inflammation. In summary, this work uncovers an auxiliary mechanism in driving lysosomal acidification, provides inspiring insights for DC biology and psoriasis etiology, and reveals SLC38A5 as a promising therapeutic target for treating psoriasis.

INTRODUCTION

Psoriasis is one of the most common chronic inflammatory skin diseases, and it induces substantial physical and psychological burdens on the affected subjects.[1–3] The etiopathogenesis of psoriasis is very complicated and involves many genetic and environmental factors, but it is well accepted that the immune system plays a key role in psoriasis.[1,4–6] The prevailing view is that skin tissue damages elicited by infection, ultraviolet radiation, or chemical reagents, among others, induce cell death and release of intracellular nucleic acids, which bind with endog-

enous antimicrobial peptides such as LL37 and form DNA(RNA)/LL37 complexes that stimulate activation of Toll-like receptors (TLRs) within dendritic cells (DCs), thus instigating production of pro-inflammatory cytokines such as interleukin-1β (IL-1β) and IL-23. The elevated production of IL-1β and IL-23 dictates activation of γδ T17 and Th17 cells and enhances the secretion of IL-17, which drives psoriatic inflammation through pleiotropic activities such as recruiting and activating neutrophils.[1,7–11] Therapeutics that specifically block IL-23 or IL-17 pathways have been approved for clinical treatment and have yielded excellent efficacy.[12–14]
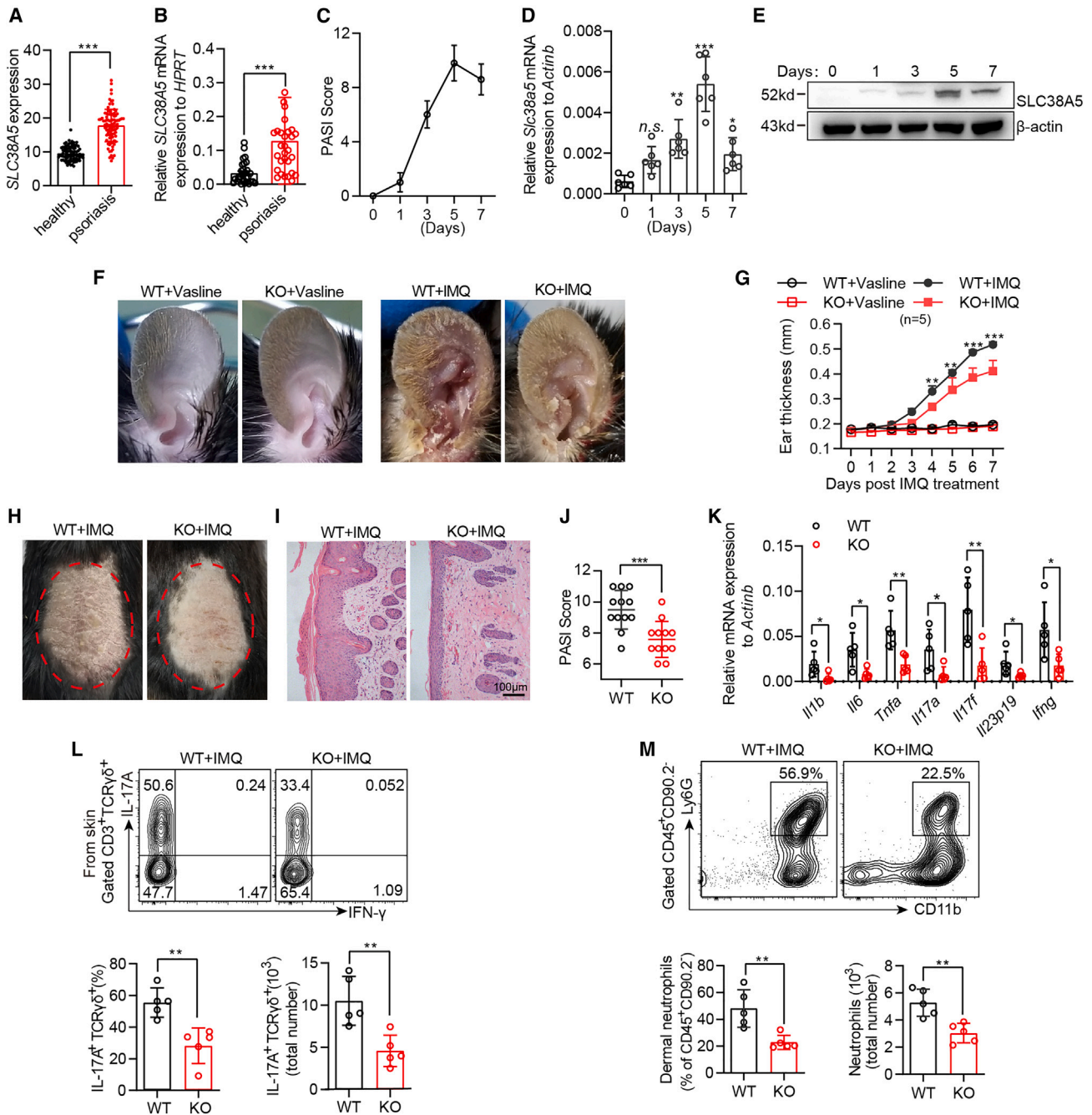
Figure 1. SLC38A5 aggravates the pathogenesis of psoriasis

(A) Publicly available dataset (GEO: GSE54456) of human patients with psoriasis (n = 92) and healthy controls (n = 82) were analyzed to compare *Slc38a5* expression in normal and psoriatic skin. Data are means ± SD.

(B) SLC38A5 mRNA expression was evaluated in skin tissue from 30 patients with psoriasis and 30 healthy controls. Data are means ± SD.

(C–E) Wild-type (WT) mice were treated with IMQ-containing cream in the right inner auricle daily for 7 consecutive days. PASI score (C), *Slc38a5* mRNA (D), and protein expression (E) in psoriatic skin was quantified at the indicated times. Data are means ± SD of six individual animals each for (C) and (D).

(F and G) WT and *Slc38a5⁻/⁻* mice were treated with 25 mg IMQ-containing cream or Vaseline cream in the right inner auricle daily for 7 consecutive days. Phenotypic presentation (F) and ear thickness of lesioned skin (G) were shown to indicate the severity of psoriasis. Data are means ± SD of five individual animals each for G.

(H–M) WT and *Slc38a5⁻/⁻* mice were treated daily with 62.5 mg IMQ-containing cream on the shaved back daily for 7 consecutive days. Clinical manifestations (H), H&E staining of the back skin (I, scale bars: 100 μm), PASI score (J), and relative expression of pro-inflammatory cytokines (K) are shown to indicate the

(legend continued on next page)

DCs play crucial roles in the pathogenesis of psoriasis.[8,9] After recognition of DNA(RNA)/LL37 complexes via TLR7, DCs phagocytize damage-associated antigens or cell debris into endosomes. These endosomes recruit and load vacuolar-type ATPase (V-ATPase) on the membrane, drive protons influx, and elicit acidification of these organelles, converting them into lysosomes that contain highly activated hydrolytic enzymes.[15–17] These enzymes digest macromolecules and make their components available to the cell as nutrients, during which they also induce cleavage and activation of TLR7, which instigates the production of pro-inflammatory cytokines such as IL-23 and IL-1β.[1,3] Topical application of imiquimod, a clinical drug for treating condyloma acuminatum, can directly bind TLR7 and induce psoriasis in both human and rodents; thus, it is the most widely accepted psoriasis model for studying the pathological mechanisms.[18,19]

Previously, we and others have revealed that multiple amino acids are involved in the pathogenesis of psoriasis through regulating immune cells or keratinocytes.[20–23] This is conceivable since psoriasis is characterized by hyperproliferation of keratinocytes and inflammatory cells, which have increased nutritional requirements.[20] These amino acids control skin homeostasis or inflammation via metabolic, epigenetic, or cellular redox pathways.[20,23] However, the details on amino acid (aa) transportation during the pathogenesis of psoriasis have not been fully elucidated.

In an analysis of aa transporters using a publicly accessible transcriptomic dataset of skin tissues from patients with psoriasis or healthy controls (GEO: GSE54456),[24] we found that *Slc38a5* (solute carrier family 38 member 5), a sodium-coupled neutral aa transporter that is responsible for transporting asparagine, glutamine, serine, glycine, or alanine across cell membranes,[25] is significantly increased in psoriatic skin. After verifying this phenomenon via our clinical human samples and mouse models, we generated a mouse strain with a deletion of the *Slc38a5* gene. SLC38A5 deficiency significantly ameliorated the pathogenesis of psoriasis, indicating a pathogenic role of this aa transporter in psoriasis. Surprisingly, SLC38A5 was almost exclusively expressed in dermal DCs when visualizing its distribution in skin tissues via laser confocal fluorescence microscopy. Further investigation confirmed that SLC38A5 mainly locates on the lysosome organelles. Mechanistically, SLC38A5 potentiates lysosomal acidification in DCs, which dictates the cleavage and activation of TLR7 with ensuing production of pro-inflammatory cytokines such as IL-23 and IL-1β and eventually aggravates psoriatic inflammation. These studies uncovered an auxiliary mechanism in driving lysosomal acidification, provided inspiring insights for the pro-inflammatory machinery of DCs and the etiology of psoriasis, and revealed SLC38A5 as a promising therapeutic target for treating psoriasis.

RESULTS

SLC38A5 aggravates the pathogenesis of psoriasis

In an attempt to study the role of aa transporters in the pathogenesis of psoriasis, we reanalyzed a publicly accessible transcriptomic dataset of skin tissues from patients with psoriasis (GEO: GSE54456)[24] and identified several upregulated aa transporters including SLC7A5 (LAT1), SLC7A1 (CAT1), and SLC6A14 (Figure S1A), which was consistent with previous reports.[20–22] Besides, we also found that *Slc38a5*, a sodium-coupled neutral aa transporter, is also significantly increased in the psoriatic skin (Figure 1A). We then recruited 30 patients with psoriasis vulgaris and 30 healthy control subjects and verified the upregulation of *Slc38a5* in the psoriatic skin (Figures 1B; Table S1). In an imiquimod (IMQ)-induced psoriasis mouse model, the expression of SLC38A5 was also increased and in parallel with the PASI (psoriasis area and severity index) score (Figures 1C–1E). These results suggested that SLC38A5 might participate in the pathogenesis of psoriasis.

Therefore, we constructed *Slc38a5* gene knockout (KO) mice (Figures S1B and S1C) to investigate its role in psoriasis. Naive SLC38A5 KO mice were normal in appearance without spontaneous morbidities or tissue inflammation (Figures S1D-S1I). However, these mice were hyposensitive to IMQ-induced psoriasis as indicated by alleviated ear swelling, attenuated PASI score, shortened rete ridges, less severe splenomegaly, ameliorated body weight loss, and reduced production of pro-inflammatory cytokines in the skin (Figures 1F–1K, S2A, and S2B). When analyzing the immune compartments, KO mice showed significantly decreased infiltration of γδ T17 and neutrophils in the skin (Figures 1L and 1M) and reduced generation of γδ T17 and Th17 cells in the spleen (Figures S2C and S2D). These findings strongly indicated that SLC38A5 aggravates the pathogenesis of psoriasis.

SLC38A5 promotes DC-mediated psoriasiform skin inflammation

To characterize the distribution of SLC38A5, we first isolated CD45^{+} immune cells and the CD45^{−} non-immune compartment from mouse skin and detected the expression of SLC38A5 via quantitative real-time PCR. The transcriptional level of *Slc38a5* in lymphocyte fraction was much higher than the non-immune compartment (Figure S3A). Then, we carried out immunofluorescent analysis of SLC38A5 in the psoriatic skin tissue of wild-type (WT) mice and used SLC38A5-KO mice as a negative control. Interestingly, SLC38A5 was barely detectable in the epidermis but showed strong signals in the dermis. Co-staining of SLC38A5 with CD11c revealed that SLC38A5 was almost exclusively expressed in CD11c^{+} dermal DCs (Figure 2A). We also co-stained SLC38A5 with langerin but did not find overlapping signals, suggesting that CD11c^{+} dermal DCs, but not Langerhans

---

severity of psoriasis. IL-17A production from skin γδ T cells (L) and the percentage and total number of neutrophils in dermal CD45^{+} CD90.2^{−} lymphocytes (M) were analyzed via fluorescence-activated cell sorting (FACS). Data are means ± SD of 12 (J) or 5 (K–M) individual animals each.

Data represent one of three independent experiments with consistent results. A two-tailed, unpaired Student's t test (A, B, and J–M), a one-way ANOVA with Sidak's multiple comparisons test (D), or a two-way ANOVA with Tukey's multiple comparisons test (G) was used to determine statistical significance (n.s., no significant difference, *p < 0.05, **p < 0.01, ***p < 0.001).
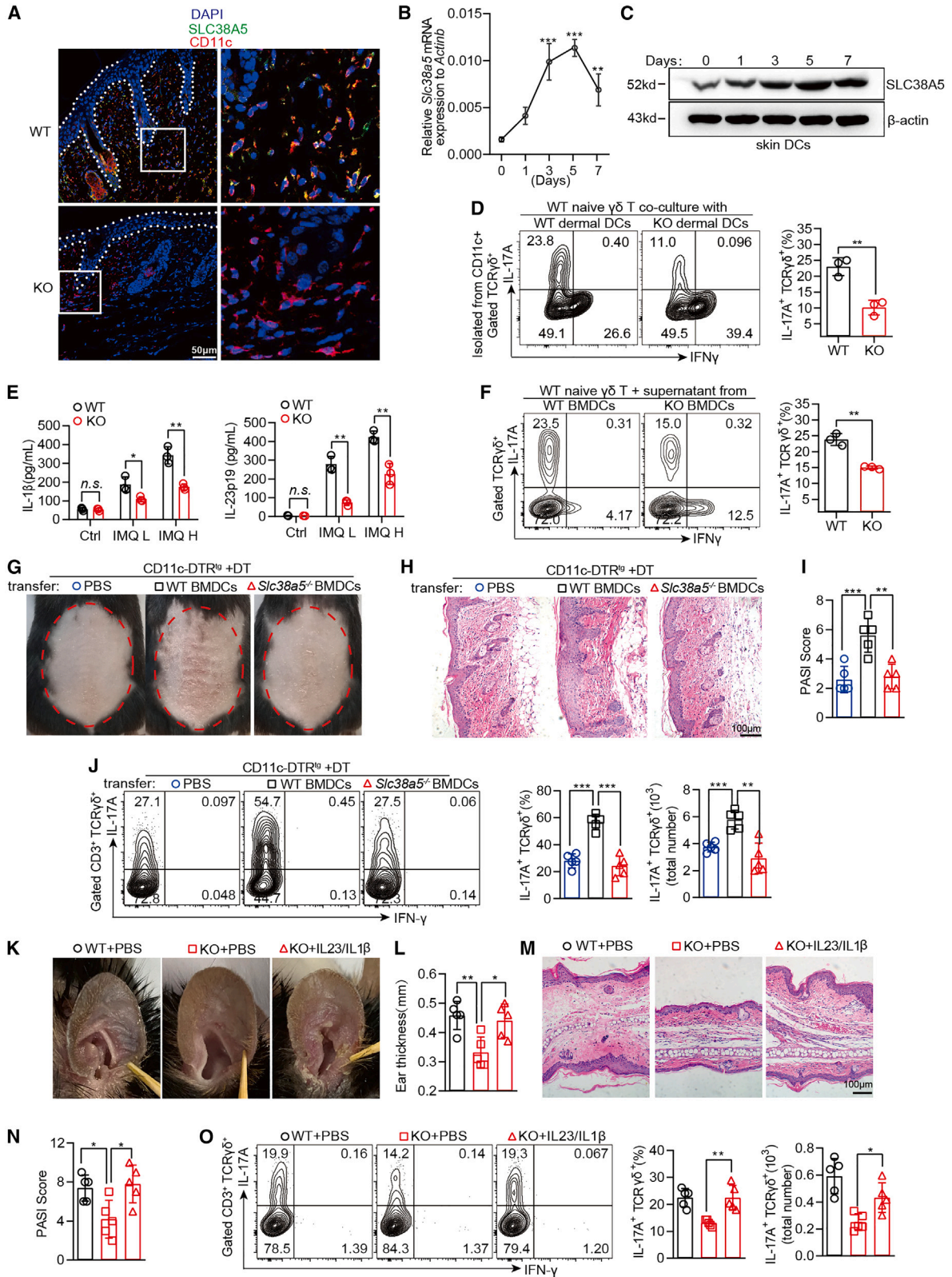
(legend on next page)

cells, were responsible for SLC38A5-mediated aggravation of psoriasis (Figure S3B). Besides, the dynamic expression of SLC38A5 in skin DCs (Figures 2B and 2C) conforms with its expression in the entire tissue (Figures 1D and 1E) and in parallel with the kinetics of the PASI score (Figure 1C). The level of SLC38A5 in skin neutrophils, however, was barely detectable during psoriasis progression (Figure S3C). In addition, compared with WT controls, DCs from the skin lesions of IMQ-treated SLC38A5-KO mice dictated less IL-17 production from $\gamma\delta$ T cells in a co-culture system (Figure 2D), which was not reproduced using lesional skin CD45$^+$ CD11c$^-$ CD11b$^+$ lymphocytes (Figure S3D). It is worth noting that the tissue residency, infiltration, and cell viability of DCs after SLC38A5 deficiency were largely unaffected (Figures S1G and S3E–S3H). These results suggested that the aggravation of psoriasis by SLC38A5 was mainly through actions in dermal DCs.

Unlike Langerhans cells that were derived from yolk sac/fatal liver, dermal DCs were continuously repopulated from bone marrow-derived precursors or monocytes.[26] Therefore, we also analyzed the expression of SLC38A5 in bone marrow-derived DCs (BMDCs), and its expression in peripheral T/B cells was checked as well. As shown in Figure S3I, SLC38A5 was barely detectable in spleen T cells or B cells but showed high levels in BMDCs. We next checked the influence of SLC38A5 deficiency on BMDCs. Indeed, SLC38A5 deficiency reduced the production of pro-inflammatory cytokines such as IL-1β and IL-23 as well as the activation of BMDCs in response to IMQ stimulation (Figures 2E and S3J–S3M), and the supernatant from these cells also dictated less IL-17 production from in-vitro-cultured $\gamma\delta$ T cells (Figure 2F), which was in accordance with lesional skin DCs (Figure 2D). Interestingly, SLC38A5 deficiency did not affect the production of IL-1β and IL-23 from cultured BMDCs in response to lipopolysaccharide (LPS) or mannose-capped lipoarabinomannan (ManLAM) (Figures S3O and S3P), suggesting a TLR-subtype-specific effect. More importantly, transferring BMDCs from SLC38A5-KO but not WT mice failed to aggravate the psoriasiform skin inflammation in DC-depleted mice recipients (Figures 2G–2J and S4A–S4F), which confirmed that SLC38A5 in bone marrow-originated DCs aggravated the

pathogenesis of psoriasis. Replenishing IL-1β and IL-23 during IMQ treatment also revived psoriasiform skin inflammation in SLC38A5-KO mice (Figures 2K–2O, S4G, and S4H), further confirming that the ameliorated psoriasis in SLC38A5-KO mice was attributed to less production of pro-inflammatory cytokines, especially IL-1β and IL-23.

Since $\gamma\delta$ T17 cells are kick starters of pro-inflammatory responses and play a critical role in psoriasis,[10,11] we also checked if SLC38A5 could affect $\gamma\delta$ T17 cells directly even though it showed much lower expression in $\gamma\delta$ T cells (Figure S3I). As expected, SLC38A5 deficiency did not affect the intrinsic differentiation ability of $\gamma\delta$ T17 cells (Figures S5A and S5B). Transferring experiments also revealed that SLC38A5 deficiency did not affect the recruitment of $\gamma\delta$ T cells or their pro-inflammatory activity (Figures S5C–S5I). These results demonstrated that SLC38A5 aggravates psoriasis via DC-generated inflammatory factors rather than directly promoting $\gamma\delta$ T 17 cells.

SLC38A5 locates in the lysosome and mediates the transportation of aas

We next examined the subcellular localization of SLC38A5 in IMQ-treated BMDCs using confocal microscopy and found that SLC38A5 was present in punctate structures and that its fluorescent signals were strongly coincided with the lysosome but not the Golgi apparatus, endoplasmic reticulum, or mitochondria (Figures 3A and 3B). We also used density-gradient ultracentrifugation to separate the subcellular compartments from mice BMDCs. Through immunoblotting analysis, we found that the majority of SLC38A5 was distributed in fraction numbers 4 and 5, in which the lysosome markers LAMP1 and LAMP2 were located (Figure 3C). These findings demonstrated that SLC38A5 was mainly located in the lysosomes. We then examined the morphology of lysosomal vesicles in fractions 4 and 5 using transmission electron microscopy, but no obvious abnormalities were discovered in the SLC38A5-deficient group (Figure 3D). In addition, no significant differences of LAMP1 and LAMP2 expression in lysosomal fraction or whole-cell lysates of BMDCs or in psoriatic skin could be found; the level of lysosomal β-galactosidase was also largely unaffected (Figures S6A–S6D),

---

Figure 2. SLC38A5 promotes DC-mediated psoriasiform skin inflammation

(A) Confocal microscopy of psoriatic lesion from WT and *Slc38a5*$^{-/-}$ mice. Slices were stained with SLC38A5 antibody (green), DC marker CD11c (red), and DAPI (blue) (scale bars: 50 μm).

(B and C) WT mice were treated with IMQ-containing cream on the back skin for 1, 3, 5, and 7 days, and skin DCs were isolated. *Slc38a5* mRNA (C) and protein expression (D) in DCs was quantified at the indicated times. Data are means ± SD of three individual animals each for (B).

(D) WT and KO mice were treated with IMQ-containing cream for 7 days, and dermal DCs were isolated and added into the culture medium of WT naive $\gamma\delta$ T cells. The production of IL-17A from $\gamma\delta$ T cells was detected and is shown. Data are means ± SD of three individual animals each.

(E) 1 × 10^6 cells of BMDCs from WT or *Slc38a5*$^{-/-}$ mice were stimulated with a low (2 μg/mL) or high (10 μg/mL) dose of IMQ for 24 h *in vitro*, and the cytokines in the supernatant were detected via ELISA. Data are means ± SD.

(F) The supernatant from *in-vitro*-cultured WT or *Slc38a5*$^{-/-}$ BMDCs pre-stimulated with IMQ was collected and added into the culture medium of WT naive $\gamma\delta$ T cells. The production of IL-17A from $\gamma\delta$ T cells was detected and is shown. Data are means ± SD of three individual animals each.

(G–J) Diphtherin (DT)-treated Itgax (CD11c)-DTR (diphtheria toxin receptor) /EGFP mice were transferred with WT or *Slc38a5*$^{-/-}$ BMDCs (PBS as negative control) and treated daily with 62.5 mg IMQ cream on the shaved back for 7 consecutive days. Representative phenotypic presentation (G), H&E staining of skin lesions (H, scale bars: 100 μm), and PASI scores (I) are shown to indicate the severity of psoriasis. IL-17A production from skin $\gamma\delta$ T cells (J) was analyzed via FACS. Data are means ± SD of five individual animals each for (I) and (J).

(K–O) Mice were injected subcutaneously with PBS or IL-23 + IL-1β in the auricle during the application of IMQ. Clinical manifestations (K), ear thickness (L), H&E staining of the auricle (M, scale bars: 100 μm), and PASI scores (N) are shown to indicate the severity of psoriasis. IL-17A production from skin $\gamma\delta$ T cells (O) was analyzed via FACS. Data are means ± SD of five individual animals each for (L), (N), and (O).

Data represent one of three independent experiments with consistent results. A two-tailed, unpaired Student's t test (D–F) or a one-way ANOVA with Sidak's multiple comparisons test (B, I, J, L, N, and O) was used to determine statistical significance (n.s., no significant difference, *p < 0.05, **p < 0.01, ***p < 0.001).

A

B

C

D

E

F
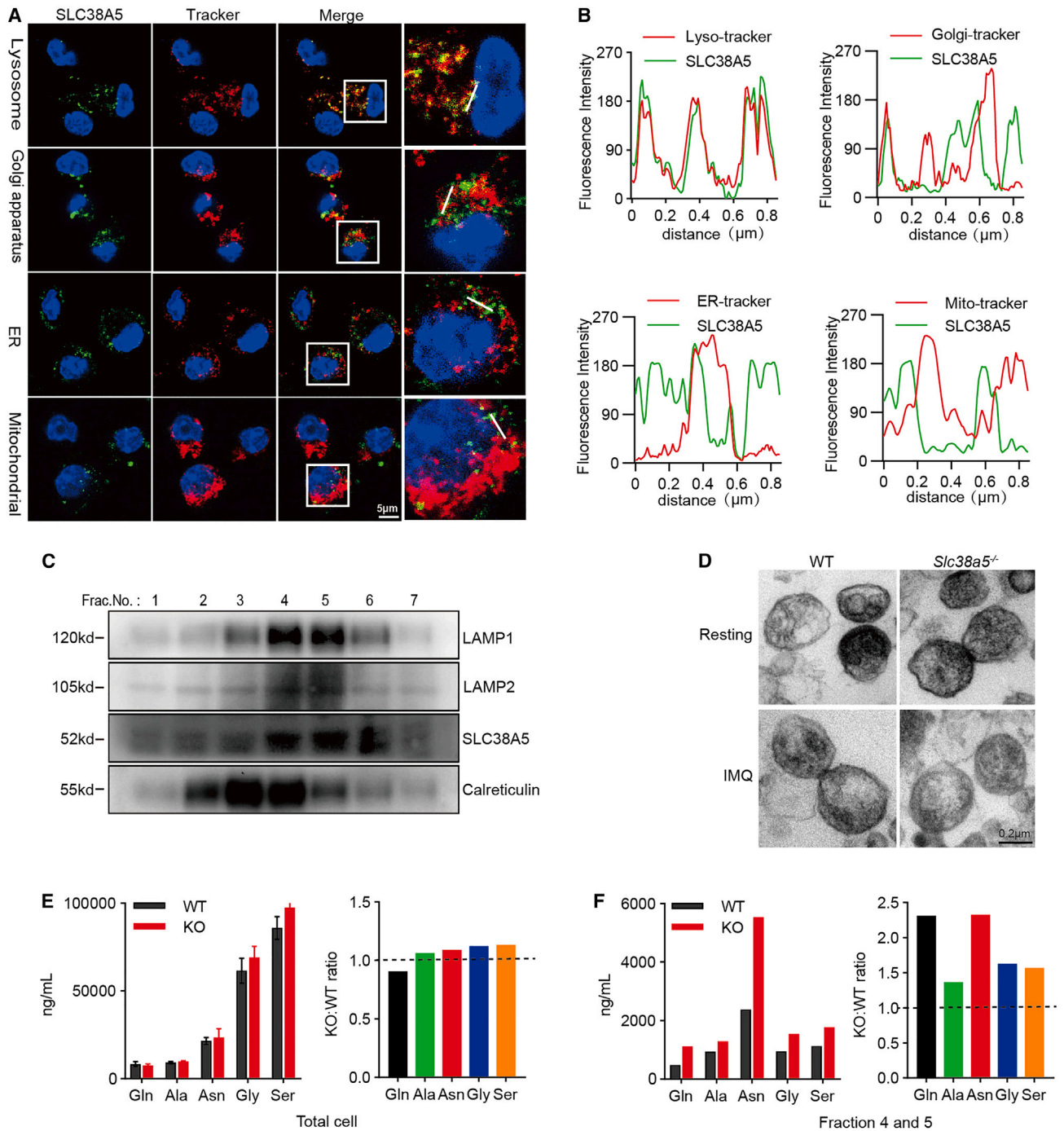
Figure 3. SLC38A5 locates in the lysosome and mediates the transportation of amino acids

(A) Confocal microscopy of the subcellular localization of SLC38A5. BMDCs were stained with organelles tracker (red), SLC38A5 antibody (green), and the DNA-binding dye DAPI (blue) before confocal microscopy. Scale bars: 5 μm.

(B) The fluorescence co-localization of SLC38A5 and subcellular organelles tracker was analyzed by ImageJ software and graphed by GraphPad Prism 8.

(C) Cell homogenates from BMDCs were separated by Opti-Prep density-gradient ultracentrifugation, and the SLC38A5, LAMP1, LAMP2, and calreticulin in each fraction was examined by western blotting.

(D) Lysosomal-rich fractions (#4 and #5) from IMQ-treated or untreated BMDCs were observed by transmission electron microscopy. Scale bars: 0.2 μm.

(E) BMDCs were treated with IMQ and total intracellular amino acid concentration was measured by liquid chromatography (LC)-MS/MS analysis. The concentration of neutral amino acids (glutamine, alanine, asparagine, glycine, serine) in WT and $Slc38a5^{-/-}$ cells and the corresponding KO vs. WT ratios are shown. Data are means ± SD.

(legend continued on next page)

which suggested that the general formation of the lysosome was largely unaffected after SLC38A5 deficiency. Since SLC38A5 is a Na$^+$-coupled transporter that co-transports sodium ions and neutral aas such as glutamine, alanine, asparagine, glycine, and serine and is coupled to H$^+$ antiporter activity,[25] we next checked if SLC38A5 deficiency affects the flux of these aas. We prepared whole-cell lysates of BMDCs or from the fractions 4 and 5 that were enriched with lysosome vesicles for free aa analysis via gas chromatography-tandem mass spectrometry (GC-MS/MS). The aas in the whole-cell lysate of KO BMDCs were comparable to WT cells; however, the concentrations of neutral aas in lysosome-enriched fractions from SLC38A5-KO BMDCs were higher than the WT group (Figures 3E, 3F, S6F, and S6G), indicating that SLC38A5 mediates the transportation of lysosomal aas in DCs.

SLC38A5 facilitates lysosome acidification and the subsequent activation of TLR7 signaling

Previous studies have demonstrated that SLC38A5 is an Na$^+$-coupled neutral aa transporter that transfers aa substrates and Na$^+$ into the cytosol while transferring H$^+$ out from the cytosol, which is an electroneutral process.[25,27] Since SLC38A5 mediates the transportation of lysosomal aas in DCs, we hypothesized that it might also facilitate the acidification of lysosome, which is critical for the activation of proteolytic enzymes that cleave and activate TLR7 with ensuing production of pro-inflammatory cytokines.[6] Therefore, we tested the acidification of lysosome in WT or SLC38A5-KO BMDCs after TLR7/IMQ engagement using a high-weight dextran (molecular weight 10,000)-conjugated lysosomal pH sensor probe, which can only enter the cell via endocytosis. As expected, the lysosomal pH in WT BMDCs decreased from 6.6 to 5.3 within 20 min of IMQ stimulation, but $Slc38a5^{-/-}$ BMDCs maintained a pH above 5.5 that could not be further acidified (Figure 4A), which was further verified using a second lysosomal pH fluorescent probe via confocal microscopy (Figure 4B). As a result, SLC38A5 deficiency significantly reduced the activation of lysosomal proteases such as asparaginyl endopeptidase (AEP; *Lgmn* for gene) or cathepsin D (CTSD) after IMQ stimulation without affecting their transcription or expression (Figures 4C–4E). The subsequent cleavage and activation of TLR7 in SLC38A5-KO BMDCs were also significantly reduced with concomitant impairment of downstream nuclear factor κB (NF-κB) and MAPK pathways[28,29] and decreased expression of pro-inflammatory cytokines (Figures 4F–4L). An interesting phenomenon is that TLR7 activation via IMQ significantly upregulated its signal transduction adaptor MyD88 and downstream signal molecule TRAF6 in WT BMDCs, indicating that the increasing cleaved TLR7 after activation has a growing demand for paired adaptors and signal transducers (Figure S7A). The expression of MyD88 and TRAF6 was largely unaffected after SLC38A5 deficiency under steady state; however, the upregulation of these molecules in SLC38A5-KO BMDCs after IMQ treatment was much less dramatic compared with WT cells (Figure S7A), which was in accordance with less

cleavage of TLR7 and less demands for paired adaptors after SLC38A5 deficiency (Figure 4F). These results indicated that SLC38A5 promotes lysosomal acidification in DCs, which dictates the activation of IMQ-TLR7 signaling pathways. Interestingly, inhibiting vacuolar-type H$^+$-ATPase,[30] the critical machinery for the acidification of lysosome,[15,31] eliminated the differences of pro-inflammatory cytokine production between WT and KO BMDCs (Figure 4I–4L and S7B–S7E), suggesting that influx of protons by SLC38A5 alone was not enough to drive the pro-inflammatory reactions by DCs and that V-ATPase still played a dominant role in these processes.

SLC38A5 facilitates lysosomal acidification and pro-inflammatory cytokine production in human DCs

The critical roles of SLC38A5 in exacerbating psoriasis, facilitating lysosomal acidification and pro-inflammatory cytokine production from DCs in the mouse model, prompted us to explore if these mechanisms also work in human DCs. Therefore, we first detected its cellular distribution in the psoriatic skin tissue of human patients. Similar to the findings made in mouse models, SLC38A5 was also mainly expressed in CD11c$^+$ DCs, and co-staining langerin, CD1c, or CD1a with SLC38A5 showed that SLC38A5 was distributed in CD1c$^+$ or CD1a$^+$ dermal DCs but not in epidermal Langerhans cells (Figure 5A). Then, we silenced SLC38A5 expression with small interfering RNA (siRNA) in human monocyte-derived DCs (Figure S8) and subjected these cells to IMQ stimulation. Consistent with findings in mice, SLC38A5 was also located in the lysosome of human DCs (Figures 5B and 5C), and its downregulation significantly reduced lysosomal acidification and AEP proteinase activity (Figures 5D and 5E). In parallel, SLC38A5 silencing in human DCs also significantly inhibited the IMQ-induced activation of NF-κB and MAPK signaling pathways (Figures 5F and 5G), as well as the production of pro-inflammatory cytokines (Figures 5H–5K). More importantly, SLC38A5 expression in human psoriatic skin tissues was also positively correlated with the PASI score and the production of pro-inflammatory cytokines such as IL-23, IL-1β, and IL-17 (Figures 5L–5O). These results strongly support the conclusion that SLC38A5 also facilitates lysosomal acidification and pro-inflammatory cytokine production in human DCs, which contributes to the pathogenesis of psoriasis.

DISCUSSION

Psoriasis is characterized by hyperproliferation of keratinocytes and inflammatory immune cells, which have increased nutritional demands.[1,20] The cell debris and damage antigens during psoriasis could be taken up, digested, and used as nutritional sources by phagocytes such as DCs; however, the orchestration process in this progress is largely unknown. Here, we found that SLC38A5, a Na$^+$-coupled neutral aa transporter, is significantly increased in psoriatic skin tissue and is almost exclusively expressed in dermal DCs when analyzing the psoriatic lesion.

(F) Lysosomal-rich fractions (#4 and #5) from IMQ treated BMDCs were subjected to LC-MS/MS analysis. The concentration of neutral amino acids in WT and $Slc38a5^{-/-}$ lysosomes and the corresponding KO vs. WT ratios are shown.

Data represent one of at least two independent experiments with consistent results.
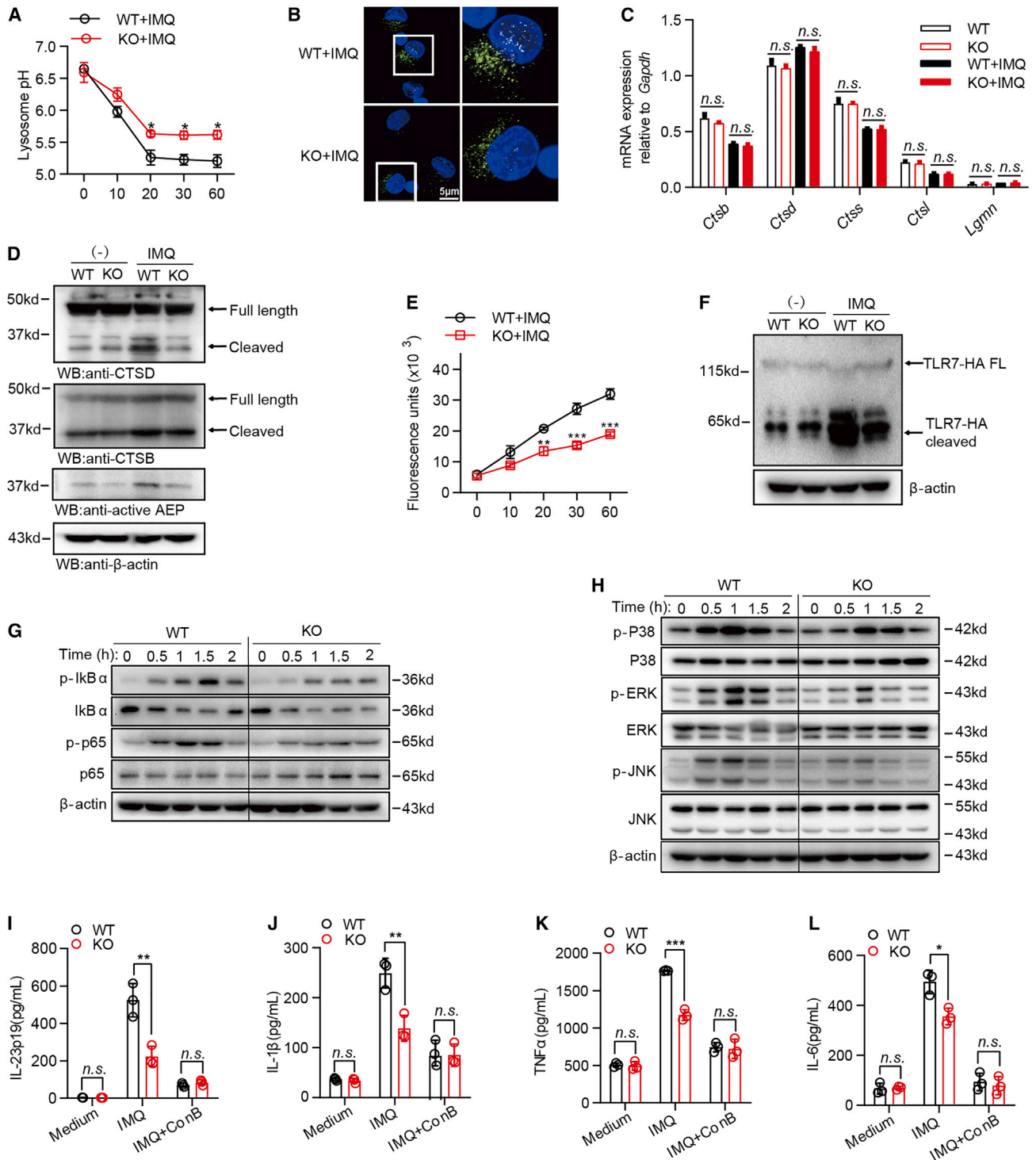
Figure 4. SLC38A5 facilitates lysosome acidification and the subsequent activation of TLR7 signaling

(A) WT or $Slc38a5^{-/-}$ BMDCs were treated with IMQ (5 μg/mL) for different times as indicated, and then the lysosomal pH in BMDCs was detected using LysoSensor Yellow/Blue dextran. Data are means ± SD.

(B) WT or $Slc38a5^{-/-}$ BMDCs were treated with IMQ (5 μg/mL) for 12 h, and then the lysosomal pH in BMDCs was detected using lysosome pH fluorescent probe by confocal microscopy. Scale bar: 5 μm.

(C) WT or $Slc38a5^{-/-}$ BMDCs were treated with IMQ (5 μg/mL) for 12 h, and then the relative mRNA expression levels of *Cathepsinb*, *Cathepsind*, *Cathepsins*, *Cathepsind*, and *Legumain* were analyzed by qPCR. Data are means ± SD.

(legend continued on next page)

Mechanically, SLC38A5 locates on the lysosome, the digestion center for endocytosed antigens, and mediates the transportation of digested neutral aas and protons between lysosomes and cytosol. As a result, SLC38A5 potentiates lysosomal acidification, which is critical for the activation of IMQ-TLR7 signaling pathways and the concomitant generation of pro-inflammatory cytokines. Therefore, the substrates being transported in both directions by SLC38A5 conspire to fuel the pro-inflammatory activities of DCs that aggravate the pathogenesis of psoriasis.

SLC38A5 is barely detectable in normal skin tissues but is significantly increased during the pathogenesis of psoriasis, and its expression level is in parallel with the PASI score (Figures 1C–1E), all of which make it a safe target for topical treatment. Besides, it is almost exclusively expressed in DCs when analyzing the psoriatic lesion (Figures 2A and 5A), suggesting that topically targeting SLC38A5 probably will not cause collateral damages to the adjacent cells or tissues. However, the mechanisms for the upregulation of SLC38A5 in psoriasis are not clear. Presumably, the excessive nutritional demands to support proliferation and the generation of cytokines might be the primordial force that propels the upregulation of SLC38A5, but the machineries that orchestrate this process still need further investigation.

Collectively, this work revealed an auxiliary mechanism in facilitating lysosomal acidification and identified SLC38A5 as an important module for the pro-inflammatory machinery of DCs and a promising target for topical treatment of psoriasis.

Limitations of the study

Since SLC38A5 mainly locates in the lysosome and facilitates lysosomal acidification in DCs, it might also participate in the epitope exposure and antigen presentation process,[32] which is critical for the generation of antigen-specific effector cells that are detrimental to psoriatic skin tissues or even healthy tissues. However, due to limited knowledge about antigen-specific effector cells in psoriasis, this work did not verify this process.

Previous studies have revealed that the transporter activity of SLC38A5 is pH dependent and that it decreases with acidification of external environment.[25,27] Therefore, the acidification of the lysosome might reduce the transporter activity of SLC38A5 in DCs. It is unclear whether a negative feedback loop of SLC38A5-mediated lysosomal acidification exists to prevent unlimited acidification and cell damage.

Another limit of this study is that we did not check whether SLC38A5 regulates the activity of V-ATPases, which might also explain the reduced lysosomal acidification and decreased inflammatory activities of SLC38A5-deficient DCs.

STAR★METHODS

Detailed methods are provided in the online version of this paper and include the following:

- KEY RESOURCES TABLE
- RESOURCE AVAILABILITY
  - Lead contact
  - Materials availability
  - Data and code availability
- EXPERIMENTAL MODEL AND STUDY PARTICIPANT DETAILS
  - Mice
  - Human subjects
- METHOD DETAILS
  - IMQ-induced psoriasis-like mouse model
  - RNA isolation, cDNA preparation, and quantitative real-time PCR (qRT-PCR)
  - Preparation of bone marrow derived DCs (BMDCs)
  - *In vitro* mouse $\gamma\delta$ T17 cell differentiation
  - Adoptive transfer of immune cells
  - Lysosomal pH measurements
  - AEP protease activity measurement
  - Intracellular vesicles isolation
  - Amino acids concentration measurement
  - Retroviral transfection of BMDCs
  - Generation of human DCs and SLC38A5 silencing
  - Skin cell preparations for flow cytometry
  - Flow cytometry (FCM)
  - Immunoblotting analysis
  - Enzyme-linked immunosorbent assay (ELISA)
  - Confocal microscopy
- QUANTIFICATION AND STATISTICAL ANALYSIS

(D) WT or $Slc38a5^{-/-}$ BMDCs were treated with or without IMQ (5 μg/mL) for 12 h, and then cathepsind, cathepsinb, and AEP protein expression was analyzed by immunoblotting.

(E) WT or $Slc38a5^{-/-}$ BMDCs were treated with IMQ (5 μg/mL) for different times as indicated, and then the AEP protease activity assays were performed. Data are means ± SD.

(F) WT or $Slc38a5^{-/-}$ BMDCs were infected with retrovirus expressing hemagglutinin (HA)-tagged TLR7 prior to treatment with IMQ (5 μg/mL). After 12 h, TLR7 cleavage was performed by western blot.

(G and H) WT or $Slc38a5^{-/-}$ BMDCs were stimulated with IMQ for different time points as indicated, and then protein expression and phosphorylation level of IκBα and p65 (G) and p38, ERK, and JNK (H) were measured by western blot.

(I–L) WT and $Slc38a5^{-/-}$ BMDCs were treated with 5 μg/mL IMQ in the presence or absence of concanamycin B (ConB; 10 ng/mL) for 24 h, and then the secretion of IL-1β, IL-23p19, tumor necrosis factor α (TNF-α), and IL-6 cytokines in supernatant was detected by ELISA. Data are means ± SD.

Data represent one of at least two independent experiments with consistent results. A two-tailed, unpaired Student's t test (I–L), a one-way ANOVA with Sidak's multiple comparisons test (C), or a two-way ANOVA with Tukey's multiple comparisons test (A and E) was used to determine statistical significance (n.s., no significant difference, *$p < 0.05$, **$p < 0.01$, ***$p < 0.001$).
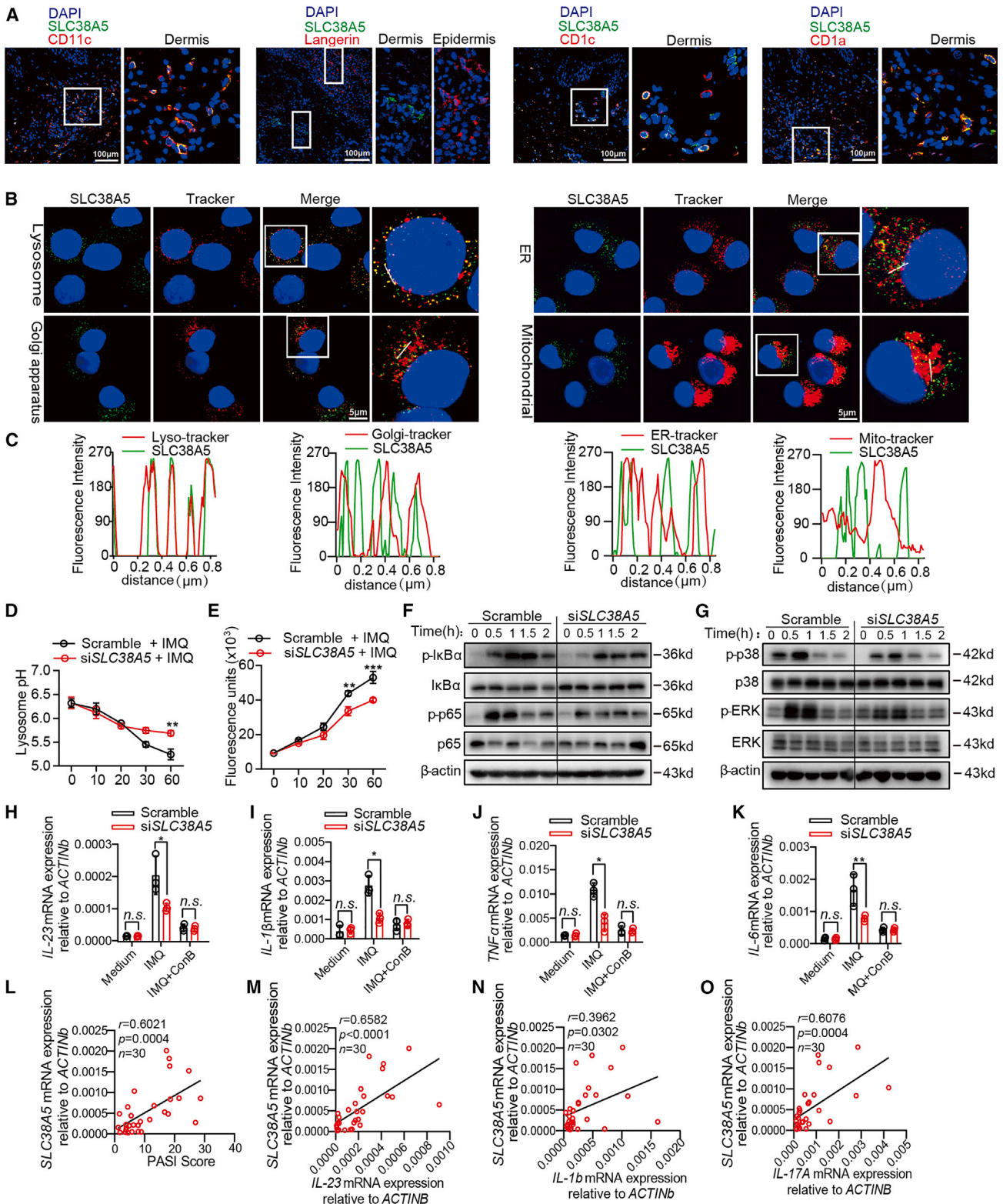
Figure 5. SLC38A5 facilitates lysosomal acidification and pro-inflammatory cytokine production in human DCs

(A) Confocal microscopy of human psoriatic lesions. Slices were stained with SLC38A5 antibody (green), DAPI (blue), and different DC markers as indicated (red). The co-staining of SLC38A5 with CD11c, CD1c, CD1a (dermal tissues), or langerin (both dermal and epidermal tissue) is shown. Scale bar: 100 μm.

(legend continued on next page)

REFERENCES

1. Griffiths, C.E.M., Armstrong, A.W., Gudjonsson, J.E., and Barker, J.N.W.N. (2021). Psoriasis. Lancet *397*, 1301–1315. https://doi.org/10.1016/S0140-6736(20)32549-6.

2. Boehncke, W.H., and Schön, M.P. (2015). Psoriasis. Lancet *386*, 983–994. https://doi.org/10.1016/S0140-6736(14)61909-7.

3. Perera, G.K., Di Meglio, P., and Nestle, F.O. (2012). Psoriasis. Annu. Rev. Pathol. *7*, 385–422. https://doi.org/10.1146/annurev-pathol-011811-132448.

4. Dainichi, T., Kitoh, A., Otsuka, A., Nakajima, S., Nomura, T., Kaplan, D.H., and Kabashima, K. (2018). The epithelial immune microenvironment (EIME) in atopic dermatitis and psoriasis. Nat. Immunol. *19*, 1286–1298. https://doi.org/10.1038/s41590-018-0256-2.

5. Bowcock, A.M., and Krueger, J.G. (2005). Getting under the skin: the immunogenetics of psoriasis. Nat. Rev. Immunol. *5*, 699–711. https://doi.org/10.1038/nri1689.

6. Lowes, M.A., Suárez-Fariñas, M., and Krueger, J.G. (2014). Immunology of psoriasis. Annu. Rev. Immunol. *32*, 227–255. https://doi.org/10.1146/annurev-immunol-032713-120225.

7. Greb, J.E., Goldminz, A.M., Elder, J.T., Lebwohl, M.G., Gladman, D.D., Wu, J.J., Mehta, N.N., Finlay, A.Y., and Gottlieb, A.B. (2016). Psoriasis. Nat. Rev. Dis. Primers *2*, 16082. https://doi.org/10.1038/nrdp.2016.82.

8. Nestle, F.O., Di Meglio, P., Qin, J.Z., and Nickoloff, B.J. (2009). Skin immune sentinels in health and disease. Nat. Rev. Immunol. *9*, 679–691. https://doi.org/10.1038/nri2622.

9. Ganguly, D., Haak, S., Sisirak, V., and Reizis, B. (2013). The role of dendritic cells in autoimmunity. Nat. Rev. Immunol. *13*, 566–577. https://doi.org/10.1038/nri3477.

10. Becher, B., and Pantelyushin, S. (2012). Hiding under the skin: Interleukin-17-producing gammadelta T cells go under the skin? Nat. Med. *18*, 1748–1750. https://doi.org/10.1038/nm.3016.

11. Papotto, P.H., Ribot, J.C., and Silva-Santos, B. (2017). IL-17(+) gammadelta T cells as kick-starters of inflammation. Nat. Immunol. *18*, 604–611. https://doi.org/10.1038/ni.3726.

12. Ghoreschi, K., Balato, A., Enerbäck, C., and Sabat, R. (2021). Therapeutics targeting the IL-23 and IL-17 pathway in psoriasis. Lancet *397*, 754–766. https://doi.org/10.1016/S0140-6736(21)00184-7.

13. Kim, J., and Krueger, J.G. (2017). Highly Effective New Treatments for Psoriasis Target the IL-23/Type 17 T Cell Autoimmune Axis. Annu. Rev. Med. *68*, 255–269. https://doi.org/10.1146/annurev-med-042915-103905.

14. Majumder, S., and McGeachy, M.J. (2021). IL-17 in the Pathogenesis of Disease: Good Intentions Gone Awry. Annu. Rev. Immunol. *39*, 537–556. https://doi.org/10.1146/annurev-immunol-101819-092536.

15. Bonam, S.R., Wang, F., and Muller, S. (2019). Lysosomes as a therapeutic target. Nat. Rev. Drug Discov. *18*, 923–948. https://doi.org/10.1038/s41573-019-0036-1.

16. Pauwels, A.M., Trost, M., Beyaert, R., and Hoffmann, E. (2017). Patterns, Receptors, and Signals: Regulation of Phagosome Maturation. Trends Immunol. *38*, 407–422. https://doi.org/10.1016/j.it.2017.03.006.

17. von Zastrow, M., and Sorkin, A. (2021). Mechanisms for Regulating and Organizing Receptor Signaling by Endocytosis. Annu. Rev. Biochem. *90*, 709–737. https://doi.org/10.1146/annurev-biochem-081820-092427.

18. Kabashima, K., and Nomura, T. (2017). Revisiting murine models for atopic dermatitis and psoriasis with multipolar cytokine axes. Curr. Opin. Immunol. *48*, 99–107. https://doi.org/10.1016/j.coi.2017.08.010.

19. Wagner, E.F., Schonthaler, H.B., Guinea-Viniegra, J., and Tschachler, E. (2010). Psoriasis: what we have learned from mouse models. Nat. Rev. Rheumatol. *6*, 704–714. https://doi.org/10.1038/nrrheum.2010.157.

20. Cibrian, D., de la Fuente, H., and Sánchez-Madrid, F. (2020). Metabolic Pathways That Control Skin Homeostasis and Inflammation. Trends Mol. Med. *26*, 975–986. https://doi.org/10.1016/j.molmed.2020.04.004.

21. Cibrian, D., Castillo-González, R., Fernández-Gallego, N., de la Fuente, H., Jorge, I., Saiz, M.L., Punzón, C., Ramírez-Huesca, M., Vicente-Manzanares, M., Fresno, M., et al. (2020). Targeting L-type amino acid transporter 1 in innate and adaptive T cells efficiently controls skin inflammation. J. Allergy Clin. Immunol. *145*, 199–214.e11. https://doi.org/10.1016/j.jaci.2019.09.025.

22. Cibrian, D., Saiz, M.L., de la Fuente, H., Sánchez-Díaz, R., Moreno-Gonzalo, O., Jorge, I., Ferrarini, A., Vázquez, J., Punzón, C., Fresno, M., et al. (2016). CD69 controls the uptake of L-tryptophan through

(B) Confocal microscopy of the subcellular localization of SLC38A5. Human monocyte-derived DCs were stained with organelle tracker (red), SLC38A5 antibody (green), and the DNA-binding dye DAPI (blue) before confocal microscopy. Scale bars: 5 μm.

(C) The fluorescence co-localization of SLC38A5 and subcellular organelles tracker was analyzed by ImageJ software and graphed by GraphPad Prism 8.

(D and E) Human monocyte-derived DCs were transfected with SLC38A5-siRNA or control siRNA and then stimulated with IMQ (5 μg/mL) for different time points as indicated. The lysosomal pHs in DCs were quantified using LysoSensor Yellow/Blue dextran (C), and the AEP protease activity assays were performed by measuring the release of fluorescent N-acetyl-methyl-coumarin (D). Data are means ± SD.

(F and G) SLC38A5-silenced monocyte-derived DCs or control cells were stimulated with IMQ for different time points as indicated, and then protein expression and phosphorylation levels of IκBα and p65 (E) and p38 and ERK (F) were measured by western blot.

(H–K) SLC38A5-silenced monocyte-derived DCs or control cells were treated with 5 μg/mL IMQ in the presence or absence of ConB (10 ng/mL) for 12 h, and then the mRNA expression levels of *IL-1β*, *IL-23p19*, *IL-6*, and *TNFα* were analyzed by qPCR. Data are means ± SD.

(L–O) Correlation of PASI score and *IL-23*, *IL-1β*, and *IL-17* mRNA expression with *SLC38A5* mRNA expression in skin lesion of patients with psoriasis (n = 30). Data represent one of at least two independent experiments with consistent results. A two-tailed, unpaired Student's t test (H–K), a Spearman's r test (L–O), or a two-way ANOVA with Tukey's multiple comparisons test (D and E) was used to determine statistical significance (n.s., no significant difference, *$p < 0.05$, **$p < 0.01$, ***$p < 0.001$).

LAT1-CD98 and AhR-dependent secretion of IL-22 in psoriasis. Nat. Immunol. *17*, 985–996. https://doi.org/10.1038/ni.3504.

23. Xia, X., Cao, G., Sun, G., Zhu, L., Tian, Y., Song, Y., Guo, C., Wang, X., Zhong, J., Zhou, W., et al. (2020). GLS1-mediated glutaminolysis unbridled by MALT1 protease promotes psoriasis pathogenesis. J. Clin. Invest. *130*, 5180–5196. https://doi.org/10.1172/JCI129269.

24. Li, B., Tsoi, L.C., Swindell, W.R., Gudjonsson, J.E., Tejasvi, T., Johnston, A., Ding, J., Stuart, P.E., Xing, X., Kochkodan, J.J., et al. (2014). Transcriptome analysis of psoriasis in a large case-control sample: RNA-seq provides insights into disease mechanisms. J. Invest. Dermatol. *134*, 1828–1838. https://doi.org/10.1038/jid.2014.28.

25. Nakanishi, T., Sugawara, M., Huang, W., Martindale, R.G., Leibach, F.H., Ganapathy, M.E., Prasad, P.D., and Ganapathy, V. (2001). Structure, function, and tissue expression pattern of human SN2, a subtype of the amino acid transport system N. Biochem. Biophys. Res. Commun. *281*, 1343–1348. https://doi.org/10.1006/bbrc.2001.4504.

26. Worbs, T., Hammerschmidt, S.I., and Förster, R. (2017). Dendritic cell migration in health and disease. Nat. Rev. Immunol. *17*, 30–48. https://doi.org/10.1038/nri.2016.116.

27. Nakanishi, T., Kekuda, R., Fei, Y.J., Hatanaka, T., Sugawara, M., Martindale, R.G., Leibach, F.H., Prasad, P.D., and Ganapathy, V. (2001). Cloning and functional characterization of a new subtype of the amino acid transport system N. Am. J. Physiol. Cell Physiol. *281*, C1757–C1768. https://doi.org/10.1152/ajpcell.2001.281.6.C1757.

28. Joosten, L.A.B., Abdollahi-Roodsaz, S., Dinarello, C.A., O'Neill, L., and Netea, M.G. (2016). Toll-like receptors and chronic inflammation in rheumatic diseases: new developments. Nat. Rev. Rheumatol. *12*, 344–357. https://doi.org/10.1038/nrrheum.2016.61.

29. Rahmani, F., and Rezaei, N. (2016). Therapeutic targeting of Toll-like receptors: a review of Toll-like receptors and their signaling pathways in psoriasis. Expert Rev. Clin. Immunol. *12*, 1289–1298. https://doi.org/10.1080/1744666X.2016.1204232.

30. Woo, J.T., Shinohara, C., Sakai, K., Hasumi, K., and Endo, A. (1992). Inhibition of the acidification of endosomes and lysosomes by the antibiotic concanamycin B in macrophage J774. Eur. J. Biochem. *207*, 383–389. https://doi.org/10.1111/j.1432-1033.1992.tb17061.x.

31. Mindell, J.A. (2012). Lysosomal acidification mechanisms. Annu. Rev. Physiol. *74*, 69–86. https://doi.org/10.1146/annurev-physiol-012110-142317.

32. Schuette, V., and Burgdorf, S. (2014). The ins-and-outs of endosomal antigens for cross-presentation. Curr. Opin. Immunol. *26*, 63–68. https://doi.org/10.1016/j.coi.2013.11.001.

STAR★METHODS

KEY RESOURCES TABLE

REAGENT or RESOURCE	SOURCE	IDENTIFIER
Antibodies		
Percp-*anti*-mouse CD3ε (Clone 145-2C11)	Biosciences	Cat# 553067; RRID: AB_394599
APC/Cyanine7 anti-mouse CD45 (Clone 30-F11)	Biosciences	Cat# 557659; RRID: AB_396774
BV500-*anti*-mouse CD90.2 (Clone 53–2.1)	Biosciences	Cat# 561616; RRID: AB_10894013
BV421 anti-mouse CD45 (Clone 30-F11)	Biolegend	Cat# 103133; RRID: AB_10899570
PE-Cy7-*anti*-mouse IFNγ (Clone XMG1.2)	Biolegend	Cat# 505826; RRID: AB_2295770
FITC-*anti*-mouse TCRγ/δ (Clone UC7-13D5)	Elabscience	Cat# E-AB-F1124C
APC-*anti*-mouse IL-17A (Clone TC11-18H10.1)	Biolegend	Cat# 506916; RRID: AB_536018
PE anti-mouse CD4 (Clone GK1.5)	Biolegend	Cat# 100408; RRID: AB_312693
PE-Cy7-*anti*-mouse CD11b (M1/70)	Biolegend	Cat# 101215; RRID: AB_312798
APC-*anti*-mouse Ly6G/Ly6C (RB6-8C5)	Biolegend	Cat# 108411; RRID: AB_313376
BV421-*anti*-mouse CD11c (N418)	Biolegend	Cat# 117329; RRID: AB_10897814
PE-*anti*-mouse Ly6C (Clone HK1.4)	Biolegend	Cat#128007; RRID: AB_1186133
FITC-*anti*-mouse F4/80 (Clone BM8)	Biolegend	Cat# 123107; RRID: AB_893500
Anti-mouse TCR γ/δ (Clone UC7-13D5)	Biolegend	Cat# 107502 RRID: AB_313311
Anti-mouse CD28 (Clone 37.51)	Sungene Biotech	Cat# M10282-14B
Anti-mouse IFN-γ (Clone XMG1.2)	Sungene Biotech	Cat# M100I16-14F
Anti-mouse SLC38A5(Clone G-7)	Santa Cruz	Cat# SC-515813
Anti-LAMP1 (C terminal)	Abcam	Cat# ab24170
Anti-LAMP2 (Clone GL2A7)	Abcam	Cat# ab13524
Anti-Calreticulin (Clone D3E6)	CST	Cat# 12238
Anti-Cathepsin D (Clone D-7)	Santa Cruz	Cat# SC377299
Anti-Cathepsin B (Clone D1C7Y)	CST	Cat# 31718
Anti-active-AEP (Clone D6S4H)	CST	Cat# 93627
Anti-Phospho-IκBα (Clone 14D4)	CST	Cat# 2859
Anti-IκBα (Clone 44D4)	CST	Cat# 4812
Anti-Phospho-p65 (Clone 93H1)	CST	Cat# 3033
Anti-p65 (Clone D14E12)	CST	Cat# 8242
Anti-Phospho-p38 (Thr180/Tyr182)	CST	Cat# 9211
Anti-p38	CST	Cat# 9212
Anti-Phospho-Erk1/2 (Thr202/Tyr204)	CST	Cat# 9101
Anti-Erk1/2	CST	Cat# 9102
Anti-Phospho-SAPK/JNK (Clone 81E11)	CST	Cat# 4668
Anti-SAPK/JNK	CST	Cat# 9252
Anti-CD1c (Clone OTI2F4)	Abcam	Cat# Ab156708
Anti-CD1a (Clone L21-A)	Abcam	Cat# Ab136922
Anti-Langerin (Clone EPR15863)	Abcam	Cat# Ab192027
Anti-β-actin (Clone 2D4H5)	Proteintech	Cat# 66009-1
Biotin conjugated anti-mouse CD11c (Clone N418)	Sungene Biotech	Cat# M10118-08B
HRP-labeled goat anti-mouse secondary antibody	Abcam	Cat# ab6789
HRP-labeled goat anti-rabbit secondary antibody	Abcam	Cat# ab6721
Alexa Fluor® 488 Goat Anti-Rabbit IgG H&L	Abcam	Cat#ab150077

Continued

REAGENT or RESOURCE	SOURCE	IDENTIFIER
Alexa Fluor® 647 Goat Anti-Mouse IgG H&L	Abcam	Cat# ab150115
Chemicals, peptides, and recombinant proteins		
Recombinant Murine IL-1b	PeproTech	Cat# 211-11B
Recombinant Mouse IL-23	Biolegend	Cat# 589002
Recombinant Murine GM-CSF	PeproTech	Cat# 315-03
Recombinant Murine IL-4	PeproTech	Cat# 214-14
Recombinant Human IL-4	PeproTech	Cat# 200-04
Recombinant Human GM-CSF	PeproTech	Cat# 300-03
Recombinant Murine IL-2	PeproTech	Cat# 212-12
Phorbol 12-myristate 13-acetate (PMA)	Sigma-Aldrich	Cat# P8139
Ionomycin	Sigma-Aldrich	Cat# I9657
Golgi-Plug	BD	Cat# 555029
Diphtherin	List Labs	Cat# 150
Nigericin	Invitrogen	Cat# N1495
Monensin	Beyotime	Cat# S1753
AEP substrate Z-Ala-Ala-Asn-AMC	Bachem	Cat# 4033201
Concanamycin B	Abcam	Cat# 144228
Opti-prep	Sigma	Cat# D1556
Lipofectamine 3000	Invitrogen	Cat# L3000-015
Collagenase IV	Sigma	Cat# C2139-1G
DNase I	Sigma	Cat# DN25-1G
TRIzol™ Reagent	ThermoFisher	Cat# 15596018
Mounting Medium With DAPI - Aqueous, Fluoroshield	Abcam	Cat# ab104139
RIPA lysis buffer	Beyotime	Cat# P0013B
EDTA-free protease inhibitor cocktail	Roche	Cat# 11697498001
Phosphatase inhibitor cocktail	Bimake	Cat# B15002
ER-Tracker Red	Beyotime	Cat# C1041
Golgi-Tracker Red	Beyotime	Cat# C1043
Mito-Tracker Red CMXRos	Beyotime	Cat# C1048B
LysoTracker red	Beyotime	Cat# C1046
ManLAM	BEI Resources	Cat# NR-14848
Critical commercial assays		
RNA Easy Fast Total RNA Extraction Kit	Tiangen Biotech	Cat# DP451;
PrimeScript RT Reagent Kit	Takara	Cat# RR037A
2× TB Green Premix Ex Taq II	Takara	Cat# RR820A
CD14 microbeads	Miltenyi Biotec	Cat# 130-050-201
LysoSensor Yellow/Blue dextran ratiometric lysosomal pH probe	Invitrogen	Cat# L22460
TM BBcellProbe Lysosome pH fluorescent probe	BestBio	BB-481215
Cytofix/Cytoperm™ Plus	BD Biosciences	Cat# 554722
ELISA MAX™ Deluxe Set Mouse TNFα	Biolegend	Cat# 430904
ELISA MAX™ Deluxe Set Mouse IL-1β	Biolegend	Cat# 432604
ELISA MAX™ Deluxe Set Mouse IL-23	Biolegend	Cat# 433704

Continued

REAGENT or RESOURCE	SOURCE	IDENTIFIER
ELISA MAX™ Deluxe Set Mouse IL-6	Biolegend	Cat# 431304
Enhanced chemiluminescence	Millipore	Cat# WBKLS050
Lysosomal β-Galactosidase staining Kit	Beyotime	Cat# C0605
BCA Protein Assay Kit	Beyotime	Cat# P0012
Deposited data		
RNA-Seq of 92 psoriatic and 82 normal skin samples	Gene Expression Omnibus (GEO)	GSE54456
Experimental models: Organisms/strains		
C57BL/6J	Jackson Laboratory	Strain #:000664, RRID:IMSR_JAX:000664
C57BL/6-$Slc38A5^{em1Smoc}$	Shanghai Model Organisms Center, Inc	Strain #: NM-KO-2114530
B6.FVB-$1700016L21$ $Rik^{Tg(Itgax-DTR/EGFP)57Lan}$/J	Jackson Laboratory	Strain #:004509 RRID:IMSR_JAX:004509
B6.129P2-$Tcrd^{tm1Mom}$/J	Jackson Laboratory	Strain #:002120 RRID:IMSR_JAX:002120
Software and algorithms		
Graghpad Prism V8	GraphPad Software	N/A
ImageJ V1.8.0	National Institutes of Health	N/A
Flowjo V10	BD	N/A

RESOURCE AVAILABILITY

Lead contact
Further information and requests for resources and reagents should be directed to and will be fulfilled by the lead contact, Zhinan Yin (tzhinan@jnu.edu.cn).

Materials availability
SLC38A5$^{-/-}$ mice were generated by our group via Shanghai Model Organisms Center, Inc. This study did not generate new unique reagents. All materials are available from the lead contact upon request.

Data and code availability
- This paper analyzes existing, publicly available data. The accession number for the dataset is listed in the key resources table. All data reported in this paper will be shared by the lead contact upon request.
- This paper does not report original code.
- Any additional information required to reanalyze the data reported in this paper is available from the lead contact upon request.

EXPERIMENTAL MODEL AND STUDY PARTICIPANT DETAILS

Mice
C57BL/6J (WT), B6.FVB-$1700016L21Rik^{Tg(Itgax-DTR/EGFP)57Lan}$/J (CD11c-DTR/EGFP) and B6.129P2-$Tcrd^{tm1Mom}$/J ($Tcrd^{-/-}$) mice were purchased from the Jackson Laboratory and maintained in our facility. C57BL/6-$Slc38A5^{em1Smoc}$ (SLC38A5-KO) mice were generated in this work via Shanghai Model Organisms Center, Inc. The animals were raised and kept in specific pathogen–free (SPF) environment at the Experimental Animal Center of the Jinan University (Guangzhou, China). The experimental protocols gained approval from the Institutional Animal Care & Use Committee (IACUC) guidelines of Jinan University.

Human subjects
30 psoriasis cases with the pathological diagnosis of psoriasis vulgaris were enrolled at the outpatient of the First Affiliated Hospital of the Jinan University. Table S1 displays the patient data. In addition, 30 healthy subjects matched for age and sex were enrolled from the medical staff of the hospital. Punch biopsy was performed to obtain psoriatic and normal skin.

Study approval. Our study protocols gained approval from the Ethics Committees of the First Affiliated Hospital of the Jinan University, and every human experiment was conducted in accordance with the guidelines of the Declaration of Helsinki. Each participant offered their written informed consent.

METHOD DETAILS

IMQ-induced psoriasis-like mouse model

Ear: IMQ cream (25 mg, Sichuan Med-shine Pharmaceuticals) or Vaseline was applied to the right inner auricle of 6-7-week-old male mice for 7 consecutive days. We determined the ear thicknesses with a slide caliper prior each application. For *in vivo* IL-23/IL-1β compensatory experiment, the $Slc38a5^{-/-}$ group was injected with 200 ng rmIL-23 (10 ng/μL) and 200 ng rmIL-1β (10 ng/μL) in 20 μL sterile PBS for 4 times at 2-day intervals during the IMQ application period. The control groups were provided with a subcutaneous injection of 20 μL sterile PBS within the auricle.

Back: IMQ cream (*62*.5 mg) was applied topically on the shaved backs of male mice (6-7-week-old) every day for 7 consecutive days.

All mice were weighed and recorded daily during the induction of psoriasis. On day 8, mice were sacrificed to collect the specimens for subsequent analyses. In histopathological examination, the tissues from each euthanized mouse were subjected to formalin fixation and paraffin embedding (FFPE), followed by slicing into 5-μm sections for HE staining. Through this work, we established an objective scoring system on the basis of patients' clinical PASI scores in order to analyze the severity of back skin inflammation in psoriasis-like mice treated with IMQ. Next, we rated erythema, thickening, and scaling on a 0–4 scale, where 0, 1, 2, 3, and 4 indicated none, mild, moderate, severe, and extremely severe state. The scores of 3 indexes were added to obtain the overall score (0–12).

RNA isolation, cDNA preparation, and quantitative real-time PCR (qRT-PCR)

TRIzol (500 μL) was used to extract the total cellular or skin tissue RNAs using the RNA Easy Fast Total RNA Extraction Kit in line with the manufacturer instructions. Later, 300–500 ng of extracted total RNAs were prepared into cDNA using the PrimeScript RT Reagent Kit through reverse transcription. Thereafter, we diluted cDNA with RNase/DNAse-free water at 1:10 to perform qRT-PCR thrice with 2× TB Green Premix Ex Taq II as per the manufacturer instruction of the CFX Connect System (Bio-Rad). For PCR, a 20-μL volume was prepared, which included 5 μL of the diluted cDNA and the reaction was performed under the following the PCR conditions: 30 s at 95°C; 5 s at 95°C, 35 s at 60°C, 15 s at 95°C, 60 s at 60°C, together with 15 s at 95°C for 45 cycles. Following every run, the melting curves were acquired for PCR products so as to adjust the gene-specific peaks and the primer dimmers. β-actin or HPRT were used as the housekeeping genes. Table S2 displays the sequences of all primers used in this work.

Preparation of bone marrow derived DCs (BMDCs)

Mouse (age 6–8 weeks, male) bone marrow was drawn from the tibias and femurs, and processed them for 3 min with the red blood cell (RBC) lysis buffer. The resultant cells were rinsed with the RPMI-1640 medium, followed by suspension and culture in the RPMI-1640 medium composed of 50 mM β-mercaptoethanol, 1% penicillin/streptomycin, 10% fetal bovine serum (FBS), 20 ng/mL rmGM-CSF, as well as 10 ng/mL recombinant mouse IL-4. At day 3 and 5, the complete RPMI-1640 medium was used to replace 1/2 of the original medium. After 7 days, we sorted the BMDCs via magnetic activated cell sorting (MACS) using the biotin conjugated anti-mouse CD11c Abs. The FACS analysis revealed that the purity of sorted DCs was >95%.

In vitro mouse γδ T17 cell differentiation

Naive γδ T-cells (CD44^{low} and CD62L^{high}) were sorted from mice spleen (age 6–8 weeks, male) via flow cytometry and the purity was validated via FACS analysis (>95%). Thereafter, the isolated cells were cultivated within the plates coated with 5 μg/mL anti–mouse γδ TCR Abs in the presence of 2 ng/mL rmIL-2 and 1 μg/mL of soluble anti–mouse CD28 Abs. In addition, we added 5 ng/mL of rmIL-1β, 5 ng/mL of rmIL-23, and 5 μg/mL of anti-mouse IFN-γ Abs as the γδ T17-skewing conditions. The cells (2.5×10^5/well, 0.5 mL) were later cultured within the 48-well plates. On day 3, the medium was refreshed and cultured for additional 3 days.

Adoptive transfer of immune cells

For the adoptive transfer of BMDCs, Itgax(CD11c)-DTR/EGFP-recipient mice (age 6–7 weeks, male) were intraperitoneally injected with 100ng diphtherin (DT) and administered with WT BMDC or $Slc38a5^{-/-}$ BMDC cells (1×10^6 cells suspended in 100 μL sterile PBS) via the ophthalmic vein. DT injection and cell transfer were performed every 3 days starting from one day prior to IMQ treatment, and 3 times of DT injection plus cell transfer were performed (Figure S4B). The mice in the control groups received injection of sterile PBS (100 μL).

For the adoptive transfer of γδ T cells, the $Tcrd^{-/-}$ mice (age 6–7 weeks, male) were administered with WT γδ T cells or $Slc38a5^{-/-}$ γδ T cells (1×10^6 cells suspended in 100 μL sterile PBS) via the ophthalmic vein every 3 days for 3 times, starting from one day prior to IMQ treatment (Figure S5C). The mice in the control group received injection of 100 μL sterile PBS.

Lysosomal pH measurements

The LysoSensor Yellow/Blue dextran ratiometric lysosomal pH probe was used for quantifying the lysosomal pH. Briefly, 1 mg/mL LysoSensor was loaded into the cells for overnight. After washing, the cells were subjected to trypsinization and PBS resuspension. Thereafter, the fluorescent microplate reader (EnSpire™ 2300 Multilabel Reader) was used to monitor fluorescence at the 340-nm excitation and 430-/535-nm emission wavelengths. The decreased 535/430 ratio suggested higher lysosomal pH (less acidic). The

cells were incubated with 10 mM nigericin/monensin contained within the MES buffer (115 mM KCL, 25 mM MES, 5 mM NaCl, and 1.3 mM $MgSO_4$) to generate the calibration curve at 10-min before the LysoSensor loading, and the pH was adjusted to 3.5–7.0. Next, we determined the 535/430 ratios for all samples. The calibration curve drawn based on MES buffer pH was used to obtain the experimental pH.

AEP protease activity measurement
The FluoStar Optima (BMG labtech) was used for analyzing the protease activity by determining the fluorescent N-acetyl-methyl-coumarin release amount within the citrate buffer (pH 5.5) under 37°C. The specific substrate for AEP (Z-Ala-Ala-Asn-AMC) was sourced from Bachem.

Intracellular vesicles isolation
The BMDCs were suspended within the extraction buffer (250 mM Sucrose, 78 mM KCl, 50 mM HEPES-OH [pH 7.5], 10 mM EGTA, 8.4 mM $CaCl_2$, 4 mM $MgCl_2$, 1× respective Halt protease/phosphatase inhibitors), followed by shear force homogenization with the 29-G syringe for fractionating the intracellular vesicles. Next, we fractionated the cell extract through 5–30% gradient ultracentrifugation with the Opti-prep at 130,000 ×g for 4 h. After separation through 4–20% SDS-PAGE, immunoblotting was conducted to confirm the fractionated vesicular proteins, followed by GC-MS/MS analyses.

Amino acids concentration measurement
GC-MS/MS analysis were performed for the measurement of the amino acids concentration. Briefly, WT and $Slc38a5^{-/-}$ BMDCs treated with or without IMQ (or lysosomes isolated from BMDCs) were deproteinized in 1 mL of pre-cooled methanol: water (V: V = 3:1) containing 0.1% formic acid, followed by sonication (500 W, 3 min, 6 s on/4 s off). Then, we added 10 μL of the internal standard (succinic acid-2,2,3,3-D4, 10 μg/mL), centrifuged it for 10 min (12000 rpm, 4°C), and then discarded the supernatant. The samples were dried with the frozen concentrator centrifugal dryer, to which 15 mg/mL of the methoxylamine hydrochloride pyridine solution was added in a volume of 80 μL to initiate the oxime reaction. Later, n-hexane (20 μL) and BSTFA-derived reagent (80 μL) that contained 1% TMCS were added, followed by vortexing for 2 min, 60 min of reaction under 70°C, and finally GC-MS/MS analysis (TSQ9000; Thermo Scientific).

Retroviral transfection of BMDCs
Tibial and femoral bone marrows were collected from the WT and KO mice (age 6–8 weeks, male), seeded in a 6-well plate, and cultivated in the RPMI-1640 medium supplemented with 10% FBS, 10 ng/mL IL-4, and 20 ng/mL GM-CSF. On day 3, 4 and 5, freshly prepared medium containing 5 μg/mL of polybrene and 50 μL of the retrovirus carrying MSCV-TLR7-HA were used to replace the original medium, followed by centrifugation at 2500 rpm and 32°C for 2 h. After removing the retroviral supernatant, the cells were resuspended with medium containing the cytokines and cultured for another 2–3 days.

Generation of human DCs and SLC38A5 silencing
Through Ficoll–Hypaque (1.077 g/mL) density-gradient centrifugation, we separated peripheral blood mononuclear cells (PBMCs) from normal blood donors. By adopting the CD14 microbeads, immunomagnetic bead selection was conducted to separate $CD14^+$ monocytes from the isolated PBMCs. For generating DCs from monocytes, we cultivated $CD14^+$ cells (1.5×10^6/mL) in the RPMI-1640 medium containing rhIL-4 and rhGM-CSF for 7 days, and the cytokines were added at 2-day intervals.

For SLC38A5 silencing, the DCs were seeded into a 6-well plate coated with the RPMI-1640 serum-free medium (2 mL) one day before transfection. Then, the mixture of siSLC38A5 or its control (scrambled siRNA) with the Lipofectamine 3000 were added into the medium at the concentration of 200 nM. After 8 h of incubation, freshly prepared medium was used to replace the original one, followed by further cell culturing for 24 h or 48 h and then collection for the subsequent experiments.

Skin cell preparations for flow cytometry
The ear or dorsal skin of the mice was cut into pieces and digested at 37°C for 1 h in 10 mL DMEM medium containing collagenase IV (1 mg/mL) and DNase I (10 μg/mL) under constant stirring. After digestion, the tissue was homogenously disaggregated using the shear force with the 29-G syringe. Then, 0.5% BSA and 5 mmol/L EDTA were added to quench the digestion enzymes. Next, we used the 70-μm nylon filter (BD Biosciences) for filtering the isolated cells and washing them with PBS containing 2% FBS for counting and FC staining.

Flow cytometry (FCM)
To stain the cell surface, we applied specific antibodies to incubate cells on an ice bath in the presence of anti-FcγR for a 15-min period to block the FcγR binding. For cytokine production analysis, we used PMA (50 ng/mL) along with ionomycin (1 μg/mL) to incubate the cells with the Golgi-Plug (1:1000) for 4 h. After stimulation, cell fixation and permeabilization with the BD Cytofix/Cytoperm Plus was performed, followed by 30-min on-ice staining with fluorescent antibodies in the dark. Each sample was obtained by the FACS Verse Flow Cytometer (BD Biosciences), followed by analysis with the FlowJo software (TreeStar).

Immunoblotting analysis

After cell collection, we used the RIPA Lysis Buffer to lyse the cells, complemented with complete EDTA-free protease inhibitor cocktail and phosphatase inhibitor cocktail. After 30-min on-ice incubation, the lysates were centrifuged for 30 min at 4 °C at the highest speed. Next, we harvested the supernatant to measure the protein levels using the BCA Protein Assay Kit. Then, we separated 20–40 μg of the total cellular proteins through 12% SDS-PAGE and adopted the PowerPac wet-blot system (Bio-Rad) to transfer proteins on the 0.22 μm PVDF membrane. After incubation with the 5% BSA blocking solution, the membranes were probed with primary antibodies at 4°C for overnight. The membranes were later rinsed for 1 h with TBST for 6 times, followed by treatment with HRP-labeled goat anti-mouse or anti-rabbit secondary antibody incubation (1:3,000) at room temperature for 2 h. Enhanced chemiluminescence was performed to collect the chemiluminescence signals on the Bio-Rad ChemiDoc MP Gel Imaging System (Bio-Rad).

Enzyme-linked immunosorbent assay (ELISA)

We harvested the supernatant medium to estimate the levels of TNFα, IL-1β, IL-6 and IL-23 levels using the ELISA kits as per the manufacturer instructions (Biolegend).

Confocal microscopy

For immunohistochemical (IHC) staining, the skin sections were deparaffinized, followed by antigen retrieval through boiling within sodium citrate (pH 6.0) and incubation with the primary antibodies (CD11c, SLC38A5) for 4 h. The sections were later rinsed with PBS thrice, followed by an additional 2 h of incubation with the Alexa Fluor 488–labeled anti–rabbit and 647–labeled anti–mouse IgG. Later, each section was rinsed thrice with PBS, followed by mounting with the DAPI-containing Fluoroshield mounting medium.

For cells immunofluorescence, BMDCs were incubated with subcellular organelle trackers (ER-Tracker Red, Golgi-Tracker Red, LysoTracker red and Mito-Tracker Red CMXRos) for 30 min (37°C) before 30 min of fixation with 4% paraformaldehyde (PFA) under ambient temperature. After 1-h of permeabilization with the blocking buffer containing 5% BSA and 0.02% Triton X-100 within PBS, the cells were subjected to 4 h incubation with the anti-SLC38A5 Abs. The cells were then rinsed with PBS thrice, followed by an additional 2 h incubation with the Alexa Fluor 488–labeled anti–rabbit IgG Abs. After washing with PBS, the DAPI-containing Fluoroshield mounting medium was used to mount the cells in the section, followed by coverslip sealing. Later, the Leica TCS SP8 confocal laser scanning microscope (Leica) was employed for image collection. The sub-organelle localization of SLC38A5 was analyzed by the ImageJ software.

QUANTIFICATION AND STATISTICAL ANALYSIS

GraphPad Prism 8.0 (GraphPad Software) was employed for statistical analyses. For normally distributed data with homogeneity of variance, the two-sided, unpaired Student's t-test was applied to compare the significant difference between the 2 groups, while that among several groups was compared by one-way analysis of variance (ANOVA). For assessment differences among groups with two independent variables, two-way ANOVA with Tukey's multiple comparisons test was also performed. For correlation analysis, linear regression analysis was performed. The sample size was not predetermined by any statistical means. The mice were accordingly randomized in diverse treatment groups. All results were represented by mean ± SD, unless specially annotated in Figure Legends. $*p < 0.05$, $**p < 0.01$, $***p < 0.001$, n.s. not significant.